Elucidating Isoniazid Resistance Using Molecular Modeling

Habibah A. Wahab,*[,†,‡] Yee-Siew Choong,[‡,§] Pazilah Ibrahim,[||] Amirin Sadikun,[||] and Thomas Scior[⊥]

Malaysian Institute of Pharmaceuticals and Nutraceuticals, Ministry of Science, Technology and Innovation, Pharmaceutical Design and Simulation Laboratory, School of Pharmaceutical Sciences, and Institute for Research in Molecular Medicine, Universiti Sains Malaysia, 11800 Minden, Malaysia, and Facultad de Ciencias Químicas, Benemérita Universidad Autónoma de Puebla, 72570 Puebla, Mexico

Received April 16, 2008

The continuing rise in tuberculosis incidence and the problem of drug resistance strains have prompted the research on new drug candidates and the mechanism of drug resistance. Molecular docking and molecular dynamics simulation (MD) were performed to study the binding of isoniazid onto the active site of *Mycobacterium tuberculosis* enoyl-acyl carrier protein reductase (InhA) in an attempt to address the mycobacterial resistance against isoniazid. Results show that isonicotinic acyl-NADH (INADH) has an extremely high binding affinity toward the wild type InhA by forming stronger interactions compared to the parent drug (isoniazid) (INH). Due to the increase of hydrophobicity and reduction in the side chain's volume of A94 of mutant type InhA, both INADH and the mutated protein become more mobile. Due to this reason, the molecular interactions of INADH with mutant type are weaker than that observed with the wild type. However, the reduced interaction caused by the fluctuation of INADH and the mutant protein only inflected minor resistance in the mutant strain as inferred from free energy calculation. MD results also showed there exists a water-mediated hydrogen bond between INADH and InhA. However, the bridged water molecule is only present in the INADH-wild type complex, reflecting the putative role of the water molecule in the binding of INADH to the wild type protein. The results support the assumption that the conversion of prodrug isoniazid into its active form INADH is mediated by KatG as a necessary step prior to target binding on InhA. Our findings also contribute to a better understanding of INH resistance in mutant type.

INTRODUCTION

Tuberculosis (TB), an infectious disease caused by *Mycobacterium tuberculosis* (MTB), is a leading killer that has plagued mankind for centuries. This disease accounts for 7% of all deaths in developing countries and as much as 26% of avoidable adult deaths.[1] One of the most effective first-line anti-TB drugs is isonicotinic acid hydrazide (INH), commonly known as isoniazid. The common therapeutics for MTB consist of a six-month regimen, using streptomycin/ethambutol in combination with INH, rifampicin, and pyrazinamide for 2 months followed by rifampicin and INH biweekly for 4 months.[2,3] During the past decade the increase in the prevalence of INH-resistant MTB strains has become a severe set back to early therapeutic success and life-threatening complication. Among new TB cases, as much as 14.1% MTB isolates are resistant to at least INH and rifampicin. The multidrug resistant (MDR) TB rate constitutes at least 5% and depends on the geographic sites.[4] Nowadays, the incidence of MDR-TB infectious is constantly rising due to the fact that TB has become a leading opportunistic infection in AIDS patients. The treatment of MDR-TB patients thus requires the administration of second line drugs (amikacin, kanamycin, capreomycin, cycloserine, *para*-aminosalicylic acid, ethionamide, and fluoroquinolones). However, these drugs are more toxic and less efficient and have a longer regiment's time. The cost of the treatment of MDR-TB is also 100 times higher than that of the basic six month short-course chemotherapy regiments.[5] Treatment for TB is more complicated and difficult with the appearance of extensively drug-resistant (EDR) TB strains[6,7] (resistant to at least INH and rifampicin and, in addition, to at least three of the six classes of second line anti-TB drugs: aminoglycosides, polypeptides, fluoroquinolones, thioamides, cycloserine, and *p*-aminosalicylic acid) since the year 2006 and the possible of extremely drug-resistant (XDR) TB strains[8] (resistant to all first- and second-line anti-TB drugs).

Koch-Weser and co-workers suggested that INH affects the MTB cell wall integrity.[9] Later reports implicated a hitherto unknown enzymatic step in the elongation and the biosynthesis of the fatty acyl chains of mycolic acids as the alleged action site of INH.[10−14] Banerjee and co-workers identified the target of INH as an *inhA* gene product.[15] The corresponding protein, namely enoyl-acyl carrier protein reductase (InhA), is involved in the synthesis of fatty acids, presumably the unique mycolic acid components of the outer mycobacterial cell. Since then, published studies have also shown InhA as the action site of INH.[16−19]

* Corresponding author phone: 604-6533888 ext 4533, 2206, 2212; fax: 604-6570017; e-mail: habibahw@usm.my, habibah@ipharm.gov.my.

† Malaysian Institute of Pharmaceuticals and Nutraceuticals, Ministry of Science, Technology and Innovation, Level 1, J05 Building, Science Complex, Universiti Sains Malaysia, 11800, Minden, Penang, Malaysia.

‡ Pharmaceutical Design and Simulation Laboratory, School of Pharmaceutical Sciences, Universiti Sains Malaysia.

§ Institute for Research in Molecular Medicine, Universiti Sains Malaysia.

|| School of Pharmaceutical Sciences, Universiti Sains Malaysia.

⊥ Benemérita Universidad Autónoma de Puebla.

10.1021/ci8001342 CCC: $40.75
Published on Web 12/10/2008

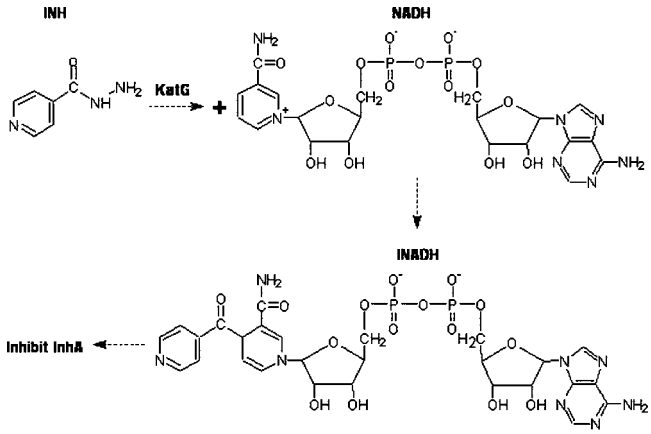

Figure 1. The flowchart of the formation of INADH.

INH-resistant MTB strains were isolated as early as 1954. Middlebrook and Winder noted a correlation between INH resistance and the loss of catalase peroxidase activity in MTB.[20,21] Later studies reported that the mutations within *katG* gene are common in INH-resistant clinical isolates, stressing the importance of KatG, a catalase-peroxidase found in MTB.[22,23] These reports suggest that INH is a prodrug which requires a *katG* gene product, KatG, in order to be activated as an anti-TB. KatG was found to be an enzyme with catalase-peroxidase activities.[24−26] Once metabolized by KatG, the activated INH metabolite reacts with NADH to form isonicotinic acyl-NADH (INADH), which is the genuine or ultimate inhibitor of InhA (Figure 1).

The INH-resistant form of MTB is related to the loss of catalase activity (KatG),[27] which is confirmed by a report that showed high level INH resistance was mainly due to the mutation(s) in *katG*.[15] Besides *katG*, other mutations in several genes of MTB are also involved in the INH resistance, which involve *inhA*, *ahpC*, *kasA*, and *ndh*.[19,28−30] The mutations within *inhA* have been reported up to 32% in INH-resistant isolates.[23,31−33] Banerjee and co-workers also showed that low-level resistance to INH in some resistant strains is associated with mutated *inhA*.[15] Mutations occurring in both *katG* and *inhA* may account for up to a total of 80% of all organisms resistant to this critical first-line anti-TB agent, whereas the mutations in *katG* alone account for the majority of INH-resistant isolates.[25,30,31,34]

In addition, literature evidence exists about INH resistance isolates with a single base change, from thymine to guanine at *inhA* nucleotide position 280 resulting in a corresponding amino acid replacement at position 94 of InhA, from serine to alanine (S94A).[35−38] Intriguingly, the location of S94A is within NADH binding region of InhA of which NADH is the cofactor,[37] which lead to the proposition that INH-resistance in S94A mutation strains is related to the reduced NADH binding affinity for InhA.[39] This proposition is supported by an X-ray crystallographic about a reduction in the hydrogen bond (Hb) network between NADH and InhA. Hence, S94A apparently results in INH resistance by preventing the inhibition of mycolic acid biosynthesis.[40]

In this study, we performed docking and molecular dynamics simulation of binding of isoniazid and its metabolite to enoyl-acyl carrier protein reductase. Both wild type and the point mutation at S94A were considered. The results of our calculations show that reduced binding affinity of the mutants S94A can be attributed to gross conformational changes of both protein and inhibitor.

METHODS

InhA System. The starting InhA coordinates were obtained from PBD. PDB id 1ZID[37] consists of wild type (WT) InhA and INADH as the ligand. The structure of the mutant (MT) was built from the WT (instead of the crystal structure of the S94A mutant deposited in the PDB as 1ENZ[41]), where the S94 of WT was mutated to A94 using *InsightII*'s Biopolymer module (Accelyrs Inc., San Diego). This was done to ensure that INADH would not be forced into the binding pocket created by NADH in the 1ENZ crystal structure.

Molecular Docking Simulation. INH coordinates were generated using *Hyperchem* 7.0 (Hypercube, Inc., Florida). The initial coordinates of INADH and NADH were obtained from PDB (the ligand of PDB id 1ZID and 1ENZ, respectively) and refined using *InsightII*'s Builder module. Ligands partial charges were assigned using *MOPAC* 6.00 (Steward, J. J., Fujitsu Limited, Tokyo) as recommended.[42] All InhA (WT and MT) were added polar hydrogen atoms using the program *protonate*, and charges were loaded using the *kollua.amber* option of *AutoDock* 3.0.5.[43] The grid maps with $90 \times 90 \times 90$ points and a spacing of 0.375 Å were generated under *AutoGrid*. The molecular docking was performed employing Lamarckian genetic algorithm (LGA) with pseudo-Solis and Wets local search and with the following parameters: population size of 50; energy evaluations of 1500000; maximum generations of 27000; translational step of 0.2 Å; orientational and torsional step of 5.0°; crossover rate of 0.80; mutation rate of 0.02; elitism of 1; local search rate of 0.06; 300 iterations per local search with termination value of 0.01; consecutive successes or failures before doubling or reducing local search step size of 4; and a total of 100 docking runs.

Molecular Dynamics (MD) Simulation. MD simulations were conducted using *Amber8*[44] with Amber 2003 force field,[45] parm99.dat parameter set,[46] TIP3P water potential parameters[47] and NPT ensembles. Periodic boundary conditions were employed with a primary cut off of 12.0 Å. Electrostatic interactions were treated using the PME method. Each complex was named after the ligand and InhA target (e.g., WT in complex with INADH is named as INADH-WT). The docking and MD starting structures of INADH-WT and MT were set up alike, while the geometry of INADH for MT was taken from the lowest docked energy conformation in the most populated cluster upon docking. Both INADH-WT and INADH-MT contain (i) one Na^+ ion as a neutralizing counterion, (ii) all water molecules from the crystal structures, and (iii) a 10 Å truncated octahedron water box. INADH-WT and INADH-MT contain 7821 and 7954 water molecules, respectively. All atoms are treated explicitly, thus INADH-WT and INADH-MT contain a total of 27559 and 27957 atoms, respectively. Each system was subsequently energy minimized under the steepest descent method followed by conjugate gradient for 1000 steps for each run. The MD parameters were as follows: 2500000 of 2 fs time step; warmed up from 0 K to and maintained at 300 K by a Berendsen thermostat[48] with the coupling constant of 0.5 ps and the SHAKE algorithm[49] was turned on throughout the simulation. A total of 200 ps were allowed

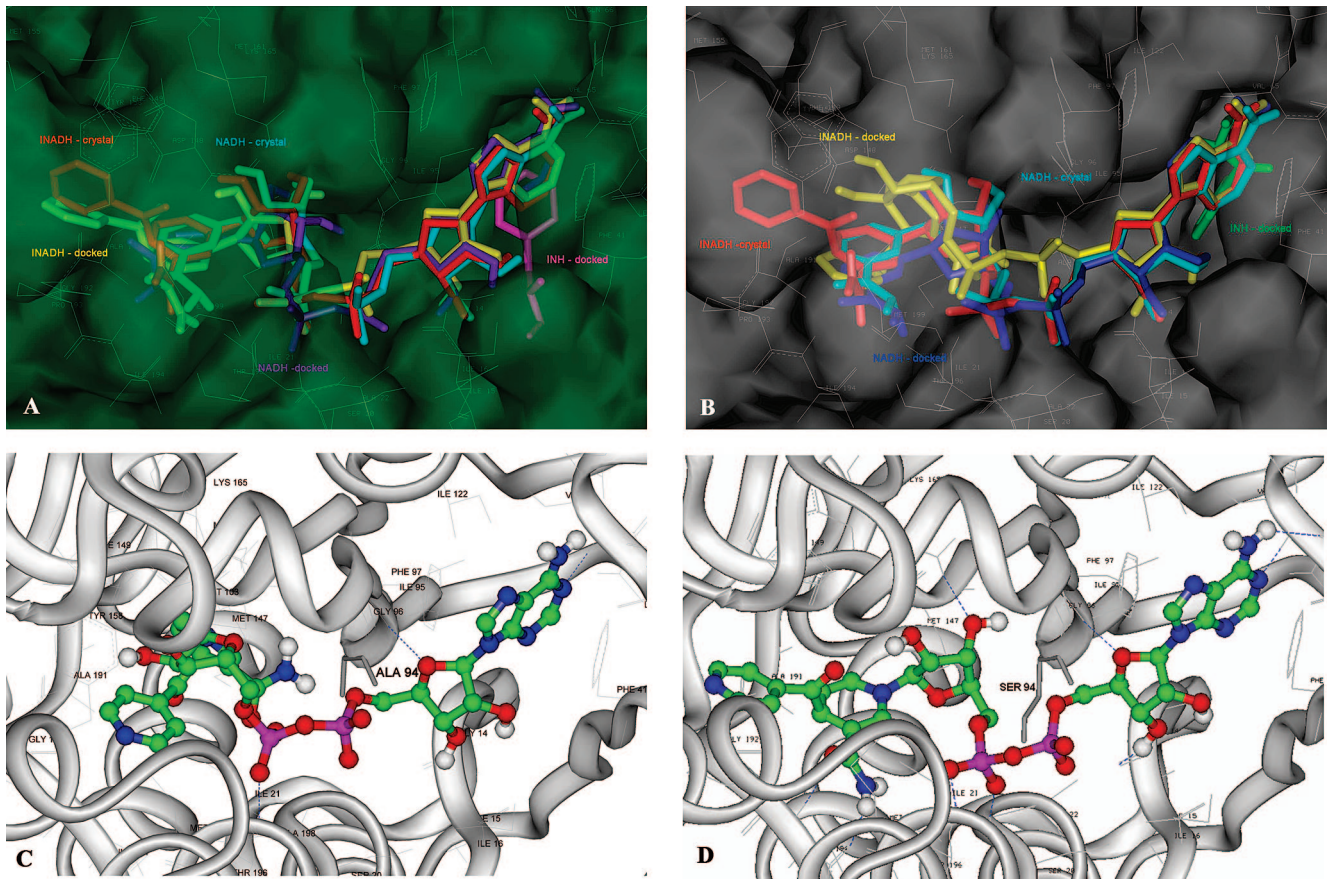

Figure 2. Docked conformations of ligands in (A) WT and (B) MT. 3-D model representation of the binding cleft (surface and line presentation) of WT and MT with the docked ligand conformations (stick presentation): INH, NADH, and INADH compared with the crystal structures (stick presentation) of NADH and INADH. Hb network (blue dotted line) between INADH (ball and stick presentation) with (C) MT and (D) WT InhA (gray ribbon presentation; stick represented S94A or S94). The *InsightII* modeling package was used to prepare these figures.

Table 1. Free Energies (ΔG) and rmsd of All Three Ligands (INH, NADH, and INADH) in WT and MT, Calculated from Docking and MD Simulations

	molecular docking		MD	
system	ΔG (kcal/mol)	rmsd (Å)	ΔG (kcal/mol)	rmsd (Å)
INADH-WT	−16.95	1.1	−14.92 ± 0.11	1.8 ± 0.2 (WT) 1.5 ± 0.2 (INADH)
INADH-MT	−12.79	1.9	−14.23 ± 0.13	2.0 ± 0.2 (MT) 2.0 ± 0.2 (INADH)
NADH-WT	−12.81	3.0	--	--
NADH-MT	−10.91	0.7	--	--
INH-WT	−5.79	--	--	--
INH-MT	−5.33	--	--	--

Table 2. Summary of Hb, Hydrophobic, van der Waals, Electrostatic, and π-π Interactions Formed by Docked Conformations of INH, NADH, and INADH in WT and MT

	number of interactions				
system	Hb	Hydrophobic	Van der Waals	Electrostatics	π-π
INH - WT	2	7	12	12	1
INH - MT	2	6	11	10	1
NADH - WT	8	15	27	26	2
NADH - MT	4	19	29	27	2
INADH - WT	9	16	29	29	4
INADH - MT	3	17	30	27	3

for the system to equilibrate, and 201−5000 ps was the production run.

RESULTS

Molecular Docking Simulation. Docking of INADH to WT and NADH to MT showed that the ligands docked in almost the same binding mode as in the crystal structure (Figure 2A,B) with the root-mean-square deviation (rmsd) of 1.1 and 0.7 Å, respectively (Table 1). Similar observation was also found where the rmsd between INADH docked into MT with the crystal structure (1ZID) is 1.9 Å (Table 1, Figure 2B).

Table 2 summarizes the interactions of ligands with WT and MT. The cutoff distance for Hydrogen bond, (Hb), hydrophobic contact, van der Waals interaction, and electrostatic interaction is 3.20 Å (angle >90−180°),[50] 4.20 Å,[51] 4.20 Å,[52] and 4.00 Å,[50] respectively. Docked NADH or INADH with WT and MT engage the same binding site (Figure 2A,B), while the ligand binding of INH to WT takes place in a different region of the binding site when compared with MT suggesting that the NADH part of INADH is crucial for binding. The results from this study extend the known conformation of INADH taken from the crystal complex with WT attesting to a clear deviation in the conformation of INADH in MT. Analyzing the docked conformations, all Hbs lie within close contact to the NADH segment of INADH. In contrast, no Hb is observed to be near to the isonicotinic acyl (pyridine ring) region. The number of Hb is reduced by INADH in complex with MT compared when compared with WT (Figure 2C,D, Table 3).

Table 3. Summary of Hbs Formed by INADH with WT and MT

system	no. of Hb	Hb donor	Hb acceptor	distance (Å)	angle (°)
INADH-WT	9	H_7 (INADH)	O (G14)	2.18	148.63
		H_N (I21)	O_6 (INADH)	2.05	165.15
		H_1 INADH)	O_{D1} (D64)	2.12	131.02
		H_N (V65)	N_2 (INADH)	2.36	147.41
		H_N (G96)	O (INADH)	1.91	170.67
		H_{Z3} (K165)	O_8 (INADH)	2.29	149.37
		H_N (I194)	O_{10} (INADH)	2.34	167.61
		H_4 INADH)	O (I194)	1.90	157.92
		H_{G1} (T196)	O_5 (INADH)	1.81	144.29
INADH-MT	3	H_N (V65)	N_2 (INADH)	1.86	164.07
		H_N (G96)	O (INADH)	2.37	170.33
		H_{G1} (T196)	O_5 (INADH)	1.81	152.42

In the case of MT, upon ligand docking the complex experienced a reduction in free binding energy (ΔG; the lowest ΔG of the most populated cluster; Table 1) compared with the WT complex ($\Delta G_{\text{INH-MT}}$: −5.33 kcal/mol; $\Delta G_{\text{INH-WT}}$: −5.79 kcal/mol; $\Delta G_{\text{NADH-MT}}$: −10.91 kcal/mol; $\Delta G_{\text{NADH-WT}}$: −12.35 kcal/mol; $\Delta G_{\text{INADH-MT}}$: −12.79 kcal/mol; $\Delta G_{\text{INADH-WT}}$: −16.95 kcal/mol). Statistically, the difference in $\Delta G_{\text{INH-WT}}$ and $\Delta G_{\text{INH-MT}}$ is not significant.

Molecular Dynamics (MD) Simulation. Analysis of the trajectories shows that the C_α atoms from WT and MT deviate at a rmsd of 1.8 ± 0.2 and 2.0 ± 0.2 Å, respectively (Table 1). Docked INADH into either WT or MT yield rmsd values of 1.5 ± 0.2 or 2.0 ± 0.2 Å, respectively (Table 1). Figure 3 represents χ_1 dihedral angle of Ala94 and S94 throughout the simulation time. Ala94's side chain was found rotating more freely during the simulation in contrast to S94's side chain's movement which was stabilized after 800 ps in INADH-WT and INADH-MT by hydrogen bonds formed by nonspecific water molecules with an occupancy ranging from 0.04−33.74%. From Table 4, the distance of INADH to S94 in WT is observed to be shorter than it is in MT, to A94 (6.07 ± 0.26 and 7.01 ± 0.76 Å for in WT and MT, respectively). Moreover, the calculated side chain volume, surface area, and hydration energy as shown in the table are all higher in S94 than A94. The $\Delta G_{\text{INADH-WT}}$ (−14.92 kcal/mol) is more negative than $\Delta G_{\text{INADH-MT}}$ (−14.23 kcal/mol) although they are comparable to the calculated values taken from molecular docking (Table 1).

Cluster analysis using MMTSB Tool Set[53] was performed to locate and cluster the similar structural conformations along the MD simulations. Only one dominant conformation for INADH-WT was observed (at 2500−5000 ps). During simulations, however, the INADH-MT complex exists in two dominant conformations, one at 800−1800 ps and another at 2700−4400 ps. Concerning INADH (Figure 4), two dominant conformations of INADH in WT were observed (at 2500−5000 ps). On the other hand, INADH in MT possesses three dominant conformations. The first and second dominant conformations were observed at 1200−2800 ps and 3000−4400 ps, respectively. The third dominant conformation was observed at 2800−3100 ps and 4100−5000 ps. The clusters conformations of INADH-WT and INADH-MT complexes did not show pronounced structural differences. However, in the case of INADH in complex with MT, obvious structural variations exist within the clusters compared to WT (Figure 5A,B). In order to describe the dynamics of INADH that leads to the structural and ΔG differences in WT and MT, we performed the analysis of the dihedral angle for the INADH main chain (Figure 6). While the dihedral angles D1, D3, D9, and D12 of INADH-MT were maintained at the same angle compared to that in WT (Figure 7), the other dihedral angles of INADH in MT were different. Thus, this might contribute to the deviation in its conformation to that WT.

The active site of InhA with INADH contains about 20 water molecules. Radial distribution function (rdf) analysis (with respect of water oxygen atom) showed that only O7 of INADH in WT has the corresponding coordination number of one, and it pronounced a sharp peak centered within 3.20 Å (cutoff distance for Hb) which integrated to the first minimum near zero (see the Supporting Information). This indicates that O7 of INADH in WT is solvated by one water molecule at almost 100% occupancy. This finding is consistent with Hb analysis (see below and Table 5). Atoms O3, O4, O6, and O10 of INADH in WT and atoms O3 and O15 of INADH in MT yield a pronounced sharp peak within 3.20 Å but with the first minimum above zero, representing a single Hb which is formed and broken between the first and second water shells. Other atoms of INADH in WT and MT presented a broad peak in the rdf plot indicating that they are almost free from solvation. The total number of water molecules around INADH within 3.20 Å was calculated as 16.1 ± 2.1 or 12.4 ± 3.2 water molecules for WT and MT, respectively. This number suggests water mediated INADH-InhA complexes. Hence, Hb analysis of INADH-InhA, INADH-water, and InhA-water complexes was conducted to identify the specific water molecule which mediated Hb of INADH and InhA. Unlike the Hb of moiety Wat275 bridging INADH (atom O7) with WT (atom H of A22), no such Hb could be found in INADH-MT (Table 5). The data concerning the average MD simulation structure (Figure 8) are concordant with rdf and Hb analysis that WT binding site is more solvated than MT site. Short-lives water mediated Hb occurred in INADH-MT, but it was formed by different water molecules which replaced each other during the simulation (data not shown). In contrast to MT, the average structure of INADH in WT shows that it is positioned at more extended conformations. Particularly, the pyridine ring of INADH in MT is slightly more squeezed at the binding site relative to WT.

DISCUSSION

Many studies postulated that INH activation by KatG is a prerequisite to the formation of INADH.[24−26] Therefore, in the case of catalytic gene *katG* mutation or absent, INH would not be metabolized by KatG. In view of these hypotheses, we conducted molecular docking and MD simulations to elucidate possible interactions of this drug or its metabolite on InhA as target molecule and thereby address the drug resistance problem. Molecular docking simulation is a well-established tool to gain insights into the ligand−receptor binding process. In principle, it is able to reproduce crystallographic data.[43,54−57] In our case, the docking was also successful and is documented by the low rmsd (1.1 Å and 0.7 Å) of the final poses measured on the bases of the original positions in the crystal structure of INADH[37] and NADH.[41] A rmsd value of less than 2.0 Å is generally an acceptable docking result when reproduction of experimental structures is concerned.[58,59] The docking experiments (100

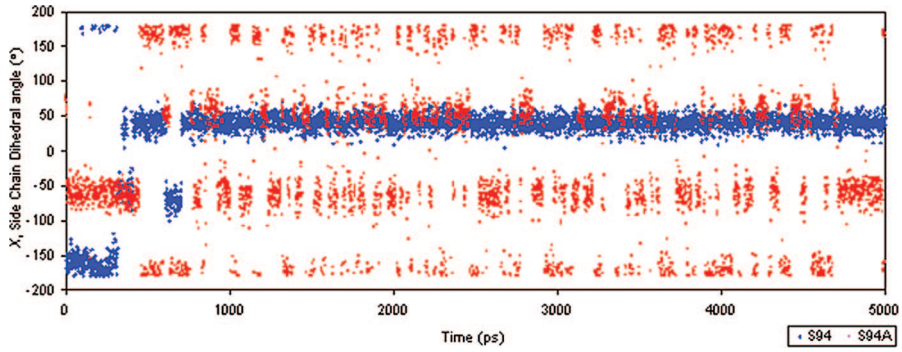

Figure 3. The χ_1 of residues 94 in WT and MT. Graphical records of χ_1 dihedral angle (torsional) angle fluctuation of S94 in WT compared with S94A in MT as a function of time during MD simulations.

Table 4. Computed Distances between INADH and Residue S94 on WT Compared with the Residue S94A on MT during MD Simulation as Well as the Calculated Properties for the Side Chains of S94 and A94 by Hyperchem 7.0

properties	amino acid S94 (WT)	S94A (MT)
distance from INADH (Å)	6.07 ± 0.26	7.01 ± 0.76
maximum distance from INADH (Å)	7.00	8.86
minimum distance from INADH (Å)	4.95	5.02
side chain volume (Å^3)	176.97	150.46
side chain approximate surface area (Å^2)	163.85	128.68
side chain hydration energy (kcal/mol)	−12.13	−1.27

unrelated runs) into the NADH binding site[41] found only one active site of InhA for all three ligands: INH, NADH and INADH, a picture which is consistent with the experimental data.

MD simulations of INADH-WT also satisfactorily reproduced the corresponding crystal structure[37] according to the rmsd measurement during simulations. Moreover, MD simulation is also a valuable tool to study the dynamical behavior of both ligand and receptor and the real solvent. The docking procedure did not handle the protein flexibility, and the solvation effect is being parametrized in the calculation where no explicit solvent is involved. The moderate fluctuation of WT and MT backbone deviation within 2.0 Å during simulation reflects that the global structure rearrangement of WT and MT is well equilibrated, maintained, and not artificially altered by the simulation. Similarly, the rmsd values for INADH in WT lie within the tolerated limits for flexible ligands simulations.[58−61] The fluctuations from crystal structure during MD simulation for INADH and INADH-InhA are expected as a result of solvated environment and a fully flexible protein. Sotriffer and co-workers suggested that the flexibility of ligand and receptor constitutes just one way to enhance affinity between the ligand and receptor.[62] In this respect, our INADH model bound to MT fluctuates stronger compared with WT. This provides clear evidence that INADH is undergoing conformational changes in order to optimize its interaction with MT. Cluster analysis revealed that INADH in MT is relatively more flexible than in WT. In fact, the intensive conformational changes of INADH in MT disturb any favorable binding to the active site and subsequently lower the binding affinity compared with WT which clearly overcome the possibility of conformational enthalpy−entropy compensation that might improve the binding free energy.

A closer inspection of the docked complex (Figure 2C-D) showed that the NADH substructure of INADH contributes 75% of the total aromatic ring-stacking (π-π) interaction for WT and MT. This observation suggests that the NADH substructure plays an essential role regarding binding affinity. The docking model also suggests that NADH is necessary to covalently bind with INH metabolite prior to its anti-TB activity. Our conclusion supports the suggestion that the mechanism of INH may be related to specific interactions between InhA and the cofactor within the NADH binding site.[41] The larger number of interactions (Hb, hydrophobic, van der Waals, electrostatic, and π-π) between INADH and WT in comparison with MT might also contribute to the more negative $\Delta G_{\text{INADH-WT}}$. Furthermore, in WT, the pyridine ring of INADH was sandwiched between A191 and F149, while the adenine moiety of INADH was sandwiched between V65 and F41. In contrast, this situation was not detected in INADH-MT. Subsequently, a stronger π-π interaction of INADH in WT than that in MT can be expected in good concordance with the studied strengthening of π-π interaction of a sandwiched aromatic ring between hydrophobic and aromatic residues.[63]

MD simulation data are in keeping with molecular docking results with regard to the INADH-InhA interaction. For instance, the pyridine ring of INADH in the INADH-WT complex (MD average geometry) is deeply buried into the WT binding pocket and surrounded by hydrophobic residues (F149, Y158, G192, L218, and W222). This favorable hydrophobic interaction is also observed in crystal structure,[37] where INADH binds stronger than NADH. This is in good agreement as obtained from docking, which showed a more negative value of ΔG_{INADH} than ΔG_{NADH}. The pyridine ring of INADH is attracted by aromatic side chains of F149, Y158, and W222. The favorable contact between the adenine ring of INADH and the benzene of F41 parallels the aforementioned π-π interaction. INADH binds better than NADH due to its pyridine ring ability to fill the cleft and form direct hydrophobic interaction with WT. This is a small but decisive difference between both residues which enables INADH to block the binding site for WT substrates (α,β-unsaturated fatty acyl chains) on WT.

S94A mutation is located in the region where the pyrophosphate group of INADH binds. The shift toward more hydrophobic side chains (S94 to A94) causes the pyrophos-

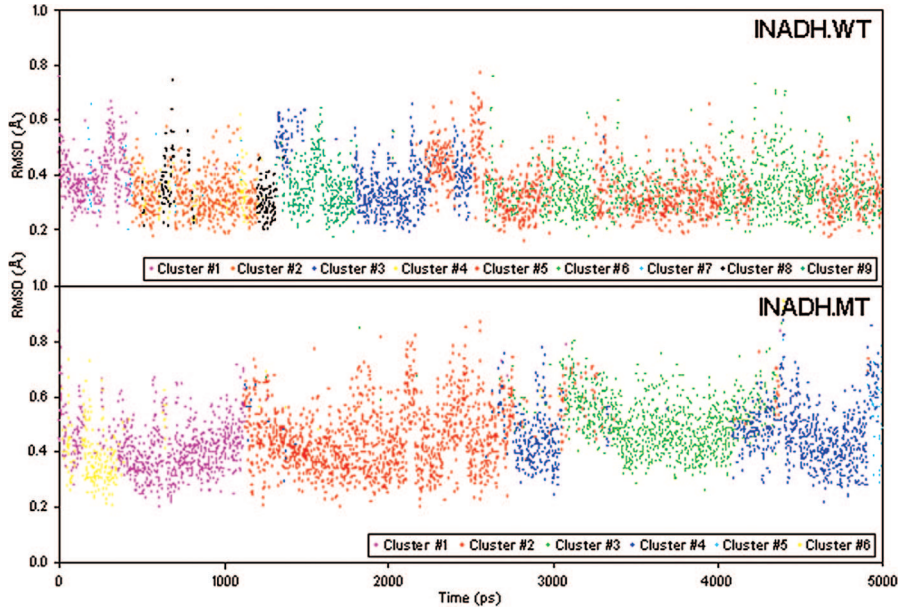

Figure 4. Diagrams of rmsd (Å) clusters of INADH in InhA (above:WT, below:MT) as a function of time. The MMTSB Tool Set was used.

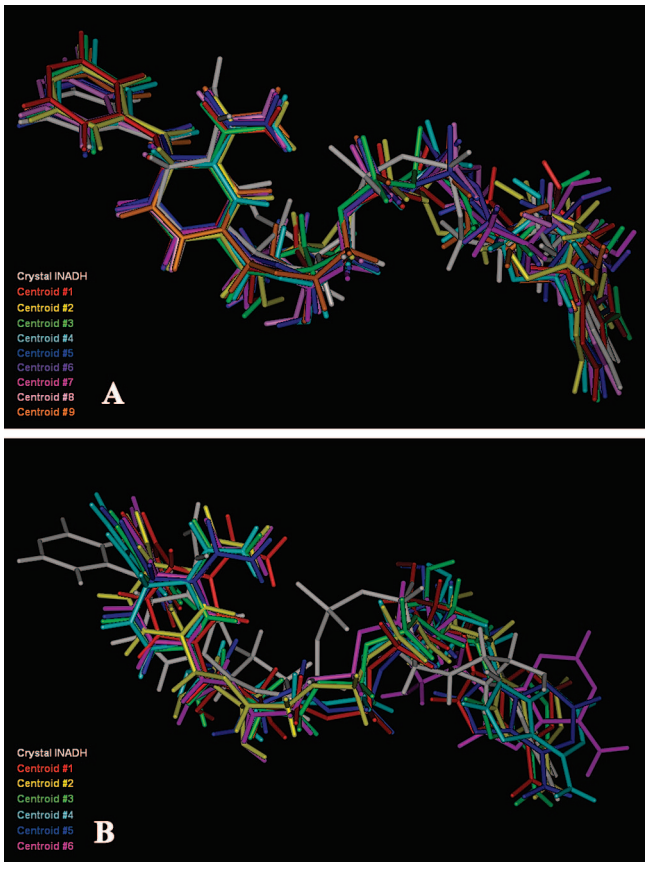

Figure 5. 3-D model representation of the final conformations with the lowest rmsd from the centroid of each cluster for INADH in WT (A) or INADH in MT (B). The *InsightII* modeling package was used.

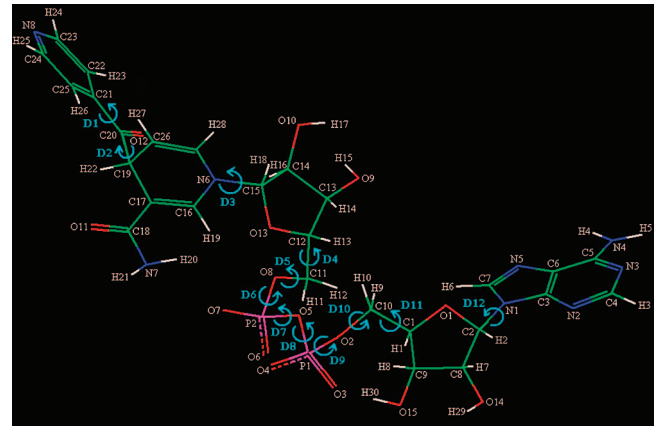

Figure 6. 3-D model representation of INADH with identification of all atoms and main chain rotational movement during MD simulations. The *InsightII* modeling package was used.

phate groups of INADH and A94 to stay away from each other, thus higher side chain fluctuation of A94 in MT than that of S94 in WT. In addition to this repulsion A94 possesses a smaller side chain than S94 where S94's side chain was able to make stronger interaction with INADH due to the smaller void from INADH. The resulting gap becomes even larger due to the repulsion of water moieties around the hydrophobic side chain of A94. As a direct consequence, both MT binding pocket and INADH find more room for conformational changes which is in full agreement with the wider fluctuation observed in the INADH-MT complex than in WT (as stated above). The gap is created at the adenine and pyridine ends of INADH and the conformational changes of INADH lead to a loss of hydrophobic and π-π interactions with the MT binding pocket. These continuous fluctuations of INADH and residues within the MT binding pocket allowed the adenine ring of INADH to move away from W222 in MT. The adenine ring of INADH in MT still in contact with F41 is not oriented toward the benzene ring of F41 as in WT, so that it can occupy a place near the entrance of the binding site of MT to expose to solvent molecules. Taken together all these factors explain the weaker π-π interaction of INADH in MT, mainly with F41 and F97. As a consequence, INADH binding to the active site residues of MT is weaker than in WT. In the same way, the pyridine of INADH does not preserve the π-π interaction with F97 as observed in WT. The acquired conformational flexibility causes not only more steric hindrance between adenine and pyridine rings of INADH but also higher intramolecular

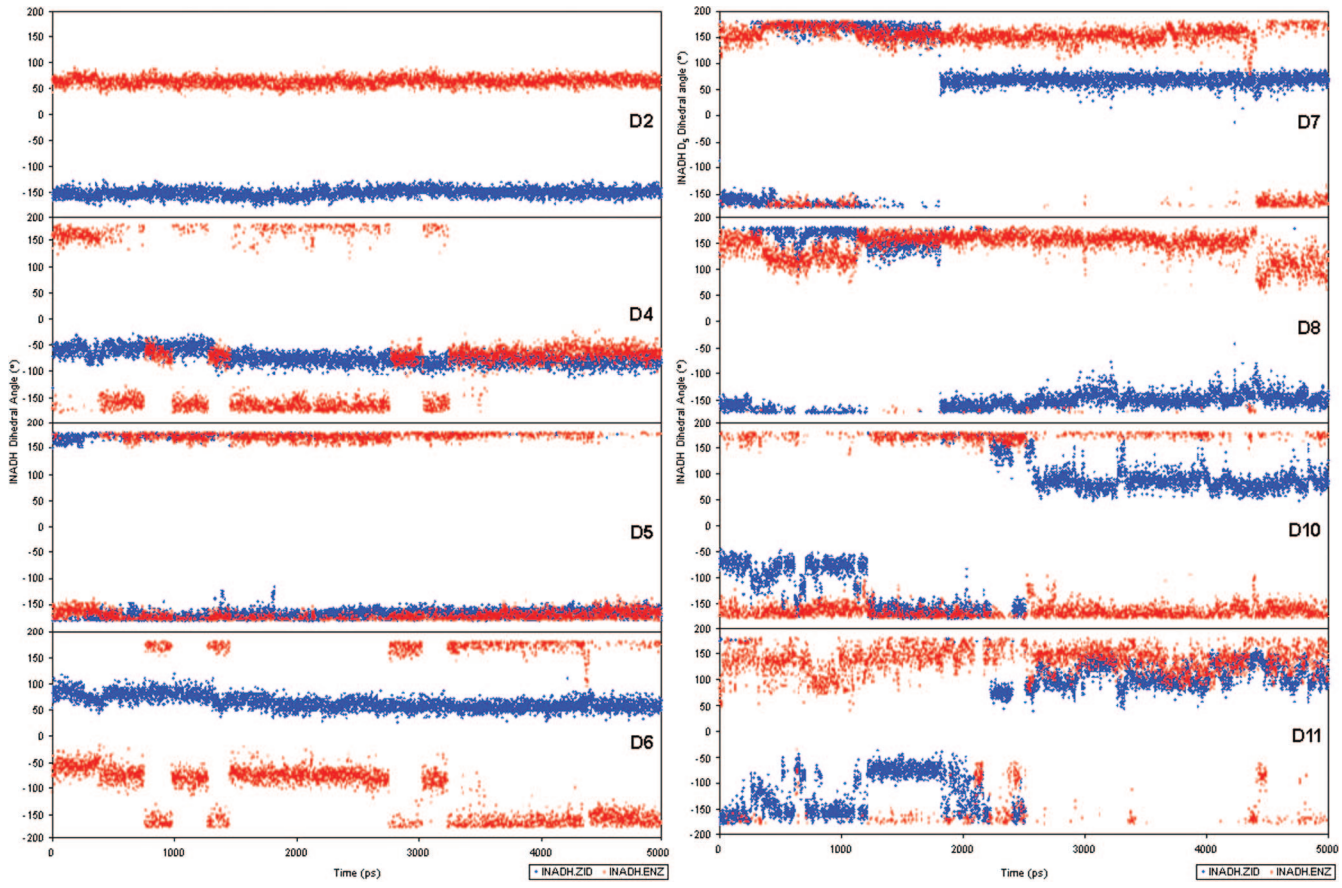

Figure 7. Graphical records of D2, D4, D5, D6, D7, D8, D10, and D11 dihedral angles on INADH (see also Figure 6) as a function of time.

Table 5. Hb Analysis in INADH-InhA Systems from MD Simulations[a]

system	occ. (%)	involved atom	distance (Å)		
			average	min.	max.
INADH-WT	99.62	O_7(INADH) - H_2(Wat275)	2.68 ± 0.12	2.38	3.19
	99.04	O_6(INADH) - H_{G1}(T196)	2.71 ± 0.13	2.39	3.20
	92.80	H(A22) - O(Wat275)	2.96 ± 0.11	2.67	3.20
	89.04	H(L196) - O(Wat300)	2.96 ± 0.11	2.61	3.20
	87.74	H(D150) - O(Wat276)	2.95 ± 0.11	2.64	3.20
	84.08	H_H(Y158) - O(Wat292)	2.81 ± 0.14	2.46	3.20
	82.28	O_{11}(INADH) - H(I194)	2.98 ± 0.12	2.61	3.20
INADH-MT	99.96	O_3(INADH) - H_G(S20)	2.61 ± 0.09	2.36	3.08
	99.80	O_4(INADH) - H_{G1}(T196)	2.63 ± 0.11	2.38	3.16
	96.12	O_6(INADH) - H(A21)	2.87 ± 0.12	2.57	3.20
	89.32	H_{D1}(H93) - O(Wat294)	2.85 ± 0.12	2.55	3.20

[a] Only the hydrogen bonds that occupied at least 80% are documented.

energies, and in its "curl-up/nonextended" conformation the ligands avoid the repulsive side chain of A94 in MT. The structural instabilities due to the fluctuation of INADH-MT are not pronounced and contributed with minor effects on the entire structure of the INADH-MT complex, to the extent the literature attests to InhA mutations with only low-level drug resistance for INH.

As the whole, our structural trajectory analyses provide a consistent molecular picture to explain the higher binding affinity of INADH in WT than in MT (in terms of ΔG). The preset structure−function relationship model is in line with the observation by Schroeder and co-workers.[64]

A closer inspection of the Hb network upon docking revealed that the conformations of INADH in MT deviate from that in the crystal structure of WT, such that I21, D64, V65, and G96 of MT have lost contact with INADH in MT compared with WT where the aforementioned amino acids are engaged in a Hb network. The reduced number of Hb contacts between NADH and MT is consistent with crystallographic results.[41] Our findings are in good agreement with docking simulations of Chen and co-workers.[65] The authors demonstrated that the different ligand affinities of NADH in WT and MT were due to structural variations.

Two Hb between INADH with WT, or three with MT, existed during the MD data collection time (at least 80% occupancy). This is significantly less than found in either crystal structures[37,41] or docking. Particularly, certain Hb seen on the INADH-InhA complex might be replaced with water

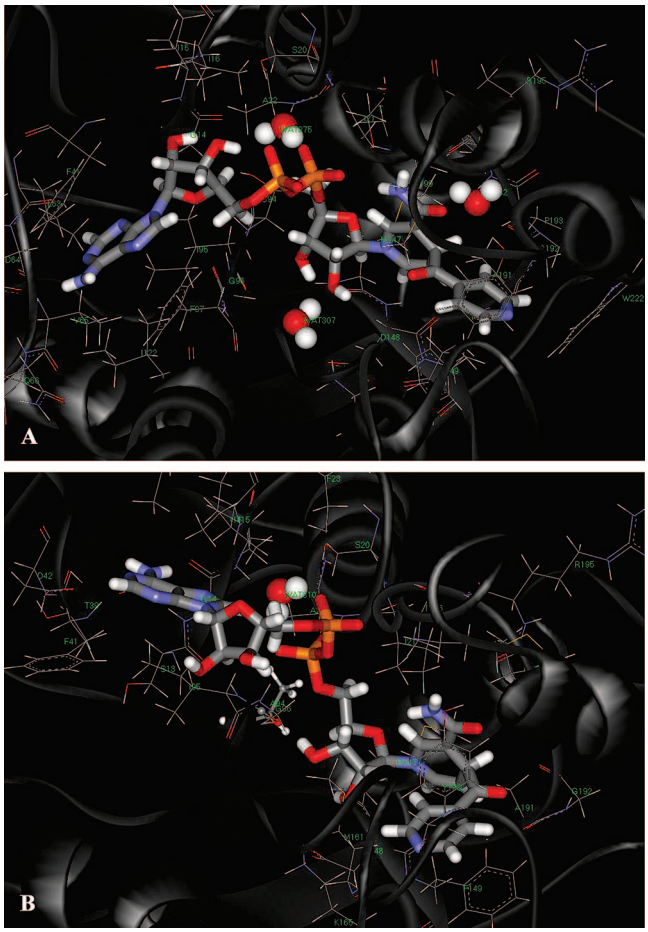

Figure 8. 3-D models of the average geometries at both binding pockets (A:WT, B:MT; ribbon models represent backbones, line models represent residues in the binding cleft, stick models represent INADH, and SPK models represent essential water molecule). The *InsightII* modeling package was used.

mediated Hb. It is even possible that such water mediated Hb take part in water exchange in concert with the solvent.

By bridging atom O7 of INADH with atom H of A22 through a Hb, Wat275 seems of paramount importance because it specifically strengthens the association of INADH with WT but not the INADH-MT complex. Water mediated Hb did occur in INADH-MT, but it was formed by different water molecules which replaced each other during the simulation, thus short-lives water mediated Hb, and did not satisfy the permanent water mediated Hb scenario as compared to the INADH-WT system. Previous studies by Pantano and co-workers did not observe Hb between NADH and WT.[66] Whether this discrepancy depends either on the different MD programs used in either research group or the fact that Pantano and co-workers[66] studied MT complexes with NADH in contrast to ours with INADH as ligand is a question that deserves further scrutiny. On the basis of the docking and MD data of this study, it becomes evident that the INADH-WT complex is more stable than NADH-WT thanks to the contribution of the 4-pyridine in INADH. INADH in WT might be more stable compared to NADH in the WT binding pocket as discussed earlier.

A closer examination of the influence of S94A mutation on the ligand binding reveals that it is by far not as obvious as expected: with only a slight difference between $\Delta G_{\text{INADH-MT}}$ and $\Delta G_{\text{NADH-MT}}$. This comparison strongly suggests that factors other than S94A mutation on InhA are important to account for the mycobacterial resistance toward INH. Despite this, the marked differences in the calculated free energies of binding of ΔG_{NADH} versus ΔG_{INH} showed that the mutation by KatG showed more resistance to INH and corroborated the known role of the cofactor NADH in NADH-dependent InhA to fulfill its enzyme activity: (i) prodrug INH can only covalently bind to NADH after its conversion into an active form by KatG and (ii) its binding to NADH only occurs in the cleft of InhA. As a consequence, MT does not directly affect INH binding itself but INH after its activation to INADH. In other words, NADH is really required for the anti-TB activity based on the results of MD and docking ΔG calculations. The results are consistent with the work of Chen and co-workers concerning NADH binding to WT and MT.[65]

The linear interaction energy (LIE) method[67] was used for MD ΔG calculation in this study as it has the advantages of i) the thermal averaging over conformations could be calculated; ii) in contrast to the FEP method,[68−70] it does not require the transformation process involving unphysical states and overcoming the limit of FEP ΔG calculation in structurally similar ligands;[71] iii) it is based on estimating the absolute binding energies where the enthalpy−entropy of solvation free energies will be canceled off;[72−74] and iv) it is slower than empirical scoring[17,52,75] of single conformations or single step perturbation technique (SSP),[76] but it is faster than FEP calculations which required higher steps number to reduce the additivity error.[77] LIE calculation of ligand binding free energies has been applied to several different systems, and the results were in good agreement with experimental data despite the difference in force fields[67,78−80] and do not need an extra preorganization term compared to the less commonly used linear response approximation (LRA).[81] Asi et al.[82] also showed that the LIE method for ligand binding free energy calculation could be applied to WT and MT *Escherichia coli* ligand-protein complexes. In this study, the calculated ΔG from MD and docking simulations were also corroborated (Table 1) despite the different methods used in their approaches: (i) united atom approximation in docking versus all atom treatment in MD, (ii) rigid versus flexible protein in docking and MD, respectively, (iii) implicit water molecules (docking) versus explicit water molecules (MD), or (iv) empirical binding free energy functions (docking) versus the semiempirical LIE method to calculate ΔG (MD).

The different mechanisms of INH activation by KatG were reviewed by Scior and co-workers.[83] In view of the fact that INH must be metabolized by mycobacterial KatG prior to its appearance as INADH with the InhA inhibitory effect, then the binding of the later to InhA must be significantly greater than the parent prodrug INH (i.e., values of ΔG must be more negative or K_i smaller). In this report, ΔG_{INADH} and ΔG_{NADH} show lower values (nearly 3-fold in the case of INADH and 2-fold for NADH) than ΔG_{INH}, indicating that INADH and NADH are a prerequisite for INH activity. It cannot be ruled out that INH may still possess anti-TB activity, though at a much lower level than in the presence of KatG, should the activation of INH not take place due to either mutation or absence of KatG. Regarding the produg

activation of INH, our data are in keeping with many experimental studies.[24−26]

CONCLUSIONS

To the best of our knowledge, this study is the first comparison between docking and MD/LIE calculated binding free energy for isonicotinic acyl-NADH (INADH) that involves wild type and mutant type enoyl-acyl carrier protein reductase (InhA). Either approach finds a higher binding affinity of INADH toward InhA than isoniazid (INH) itself. The consistent results support the idea of INH activation by forming INADH, which in turn possesses a higher affinity to InhA than INH. On a molecular basis the observed INH resistance through S94A mutation is explained by a weaker binding strength of mutant with INADH than with NADH because the latter can compete successfully with the former replacing it on InhA and thereby unblocking this target enzyme so that *M. tuberculosis* can survive. Since the binding affinity of INADH and NADH with InhA are much greater than INH, it clearly supports the suggestion that S94A mutation results in low level INH resistance. The view held by others that the activation role of KatG is a prerequisite is fully compatible with our combined *in silico* approaches. The ligand was optimized by evolution to have favorable interaction free energy of binding with wild type protein. Thte mutant protein has more pronounced flexibility giving rise to decreased affinity toward inhibitor. The design of novel inhibitors that remains a challenge for the future involves protein engineering in terms of structure and flexibility. This study confirms and expands the hitherto known facts on INH resistance on a molecular scale and may contribute in anti-TB drug discovery programs which can be used for predicting the new anti-TB agents with novel molecular mechanisms of action.

ACKNOWLEDGMENT

This work was supported by a USM short-term grant (grant no.: 304/PFARMASI/633069). We thank MIMOS for providing the computing time for this work. Our gratitude is also extended to CONACYT (2007-52639) for the support.

Supporting Information Available: The radial distribution function, $g(r)$, and the corresponding integration numbers, $n(r)$, from the hydrogen bond acceptor atom of INADH to the oxygen atom of water molecules. This material is available free of charge via the Internet at http://pubs.acs.org.

REFERENCES AND NOTES

(1) Gomez, J. E.; McKinney, J. D. *M. tuberculosis* persistence, latency, and drug tolerance. *Tuberculosis (Edinb)* **2004**, *84*, 29–44.
(2) Bass, J. B.; Farer, L. S.; Hopewell, P. C.; O'Brien, R.; Jacobs, R. F.; Ruben, F.; Snider, D. E.; Thornton, G. Treatment of tuberculosis and tuberculosis Infection in adults and children. *Am. J. Respir. Crit. Care Med.* **1994**, *149*, 1359–1374.
(3) Iyawoo, K. Tuberculosis in Malaysia: problems and prospect of treatment and control. *Tuberculosis* **2004**, *84*, 4–7.
(4) Yam, W. C.; Tam, C. M.; Leung, C. C.; Tong, H. L.; Chan, K. H.; Leung, E. T.; Wong, K. C.; Yew, W. W.; Seto, W. H.; Yuen, K. Y.; Ho, P. L. Direct detection of rifampin-resistant *Mycobacterium tuberculosis* in respiratory specimens by PCR-DNA sequencing. *J. Clin. Microbiol.* **2004**, *42*, 4438–4443.
(5) Pablos-Mendez, A.; Gowda, D. K.; Frieden, T. R. Controlling multidrug-resistant tuberculosis and access to expensive drugs: a rational framework. *Bull. World Health Org.* **2002**, *80*, 489–495.
(6) Gandhi, N. R.; Moll, A.; Sturm, A. W.; Pawinski, R.; Govender, T.; Lalloo, U.; Zeller, K.; Andrews, J.; Friedland, G. Extensively drug-resistant tuberculosis as a cause of death in patients co-infected with tuberculosis and HIV in a rural area of South Africa. *Lancet* **2006**, *368*, 1575–1580.
(7) Shah, N. S.; Wright, A.; Bai, G. H.; Barrera, L.; Boulahbal, F.; Martin-Casabona, N.; Drobniewski, F.; Gilpin, C.; Havelková, M.; Lepe, R.; Lumb, R.; Metchock, B.; Portaels, F.; Rodrigues, M. F.; Rüsch-Gerdes, S.; Van Deun, A.; Vincent, V.; Laserson, K.; Wells, C.; Cegielski, J. P. Worldwide emergence of extensively drug-resistant tuberculosis. *Emerging Infect. Dis.* **2007**, *13*, 380–387.
(8) Migliori, G. B.; Loddenkemper, R.; Blasi, F.; Raviglione, M. C. 125 years after Robert Koch's discovery of the tubercle bacillus: the new XDR-TB threat. Is "science" enough to tackle the epidemic. *Eur. Respir. J.* **2007**, *29*, 423–427.
(9) Koch-Weser, D.; Ebert, R. H.; Barclay, W. R.; Lee, V. S. Studies on the metabolic significance of acid-fastness of tubercle bacilli. *J. Lab. Clin. Med.* **1953**, *42*, 828–829.
(10) Winder, F. G.; Collins, P. B. Inhibition by isoniazid of synthesis of mycolic acids in *Mycobacterium tuberculosis*. *J. Gen. Microbiol.* **1970**, *63*, 41–48.
(11) Takayama, K.; Wang, L.; David, H. L. Effect of isoniazid on the in vivo mycolic acid synthesis, cell growth, and viability of. *Mycobacterium tuberculosis. Antimicrob. Agents Chemother.* **1972**, *2*, 29–35.
(12) Davidson, L. A.; Takayama, K. Isoniazid inhibition of the synthesis of monounsaturated long-chain fatty acids in *Mycobacterium tuberculosis* H37Ra. *Antimicrob. Agents Chemother.* **1979**, *16*, 104–105.
(13) Kikuchi, S.; Takeuchi, T.; Yasui, M.; Kusaka, T.; Kolattukudy, P. E. A very long-chain fatty-acid elongation system in *Mycobacterium avium* and a possible mode of action of isoniazid on the system. *Agric. Biol. Chem.* **1989**, *53*, 1689–1698.
(14) Quemard, A.; Lacave, C.; Laneelle, G. Isoniazid inhibition of mycolic acid synthesis by cell extracts of sensitive and resistant strains of *Mycobacterium Aurum*. *Antimicrob. Agents Chemother.* **1991**, *35*, 1035–1039.
(15) Banerjee, A.; Dubnau, E.; Quemard, A.; Balasubramanian, V.; Um, K. S.; Wilson, T.; Collins, D.; de Lisle, G.; Jacobs, W. R., Jr. *inhA*, a gene encoding a target for isoniazid and ethionamide in *Mycobacterium tuberculosis*. *Science* **1994**, *263*, 227–230.
(16) Telenti, A.; Honore, N.; Bernasconi, C.; March, J.; Ortega, A.; Heym, B.; Takiff, H. E.; Cole, S. T. Genotypic assessment of isoniazid and rifampin resistance in *Mycobacterium tuberculosis*: a blind study at reference laboratory level. *J. Clin. Microbiol.* **1997**, *35*, 719–723.
(17) Wang, J. Y.; Burger, R. M.; Drlica, K. Role of superoxide in catalase-peroxidase-mediated isoniazid action against mycobacteria. *Antimicrob. Agents Chemother.* **1998**, *42*, 709–711.
(18) Fang, Z.; Doig, C.; Rayner, A.; Kenna, D. T.; Watt, B.; Forbes, K. J. Molecular evidence for heterogeneity of the multiple-drug-resistant *Mycobacterium tuberculosis* population in Scotland (1990 to 1997). *J. Clin. Microbiol.* **1999**, *37*, 998–1003.
(19) Vilcheze, C.; Morbidoni, H. R.; Weisbrod, T. R.; Iwamoto, H.; Kuo, M.; Sacchettini, J. C.; Jacobs, W. R., Jr. Inactivation of the *inhA*-encoded fatty acid synthase II (FASII) enoyl-acyl carrier protein reductase induces accumulation of the FASI end products and cell lysis of *Mycobacterium smegmatis*. *J. Bacteriol.* **2000**, *182*, 4059–4067.
(20) Middlebrook, G. Isoniazid-resistance and catalase activity of tubercle bacilli; a preliminary report. *Am. Rev. Tuberc.* **1954**, *69*, 471–472.
(21) Winder, F. Catalase and peroxidase in mycobacteria. Possible relationship to the mode of action of isoniazid. *Am. Rev. Respir. Dis.* **1960**, *81*, 68–78.
(22) Stoeckle, M. Y.; Guan, L.; Riegler, N.; Weitzman, I.; Kreiswirth, B.; Kornblum, J.; Laraque, F.; Riley, L. W. Catalase-peroxidase gene sequences in isoniazid-sensitive and -resistant strains of *Mycobacterium tuberculosis* from New York City. *J. Infect. Dis.* **1993**, *168*, 1063–1065.
(23) Heym, B.; Alzari, P. M.; Honore, N.; Cole, S. T. Missense mutations in the catalase-peroxidase genekatG, are associated with isoniazid resistance in *Mycobacterium tuberculosis*. *Mol. Microbiol.* **1995**, *15*, 235–245.
(24) Zhang, Y.; Dhandayuthapani, S.; Deretic, V. Molecular basis for the exquisite sensitivity of *Mycobacterium tuberculosis* to isoniazid. *Proc. Natl. Acad. Sci. U.S.A.* **1996**, *93*, 13212–6.
(25) Cynamon, M. H.; Zhang, Y.; Harpster, T.; Cheng, S.; DeStefano, M. S. High-dose isoniazid therapy for isoniazid-resistant murine *Mycobacterium tuberculosis* infection. *Antimicrob. Agents Chemother.* **1999**, *43*, 2922–2924.
(26) Lei, B.; Wei, C. J.; Tu, S. C. Action mechanism of antitubercular isoniazid Activation by *Mycobacterium tuberculosis* KatG, isolation, and characterization of InhA inhibitor. *J. Biol. Chem.* **2000**, *275*, 2520–2526.

(27) Zhang, Y.; Heym, B.; Allen, B.; Young, D.; Cole, S. The catalase-peroxidase gene and isoniazid resistance of *Mycobacterium tuberculosis*. *Nature* **1992**, *358*, 591–593.
(28) Piatek, A. S.; Telenti, A.; Murray, M. R.; El-Hajj, H.; Jacobs, W. R., Jr.; Kramer, F. R.; Alland, D. Genotypic analysis of *Mycobacterium tuberculosis* in two distinct populations using molecular beacons: implications for rapid susceptibility testing. *Antimicrob. Agents Chemother.* **2000**, *44*, 103–110.
(29) Slayden, R. A.; Barry, C. E. 3rd, The genetics and biochemistry of isoniazid resistance in *Mycobacterium tuberculosis*. *Microbes. Infect.* **2000**, *2*, 659–669.
(30) Torres, M. J.; Criado, A.; Palomares, J. C.; Aznar, J. Use of real-time PCR and fluorimetry for rapid detection of rifampin and isoniazid resistance-associated mutations in *Mycobacterium tuberculosis*. *J. Clin. Microbiol.* **2000**, *38*, 3194–3199.
(31) Morris, S.; Bai, G. H.; Suffys, P.; Portillo-Gomez, L.; Fairchok, M.; Rouse, D. Molecular mechanisms of multiple drug resistance in clinical isolates of *Mycobacterium tuberculosis*. *J. Infect. Dis.* **1995**, *171*, 954–960.
(32) Lee, A. S.; Lim, I. H.; Tang, L. L.; Telenti, A.; Wong, S. Y. Contribution of *kasA* analysis to detection of isoniazid-resistant *Mycobacterium tuberculosis* in Singapore. *Antimicrob. Agents Chemother.* **1999**, *43*, 2087–2089.
(33) Kiepiela, P.; Bishop, K. S.; Smith, A. N.; Roux, L.; York, D. F. Genomic mutations in the *katG*inhA and aphC genes are useful for the prediction of isoniazid resistance in Mycobacterium tuberculosis isolates from Kwazulu Natal, South Africa. *Tuber. Lung Dis.* **2000**, *80*, 47–56.
(34) Musser, J. M.; Kapur, V.; Williams, D. L.; Kreiswirth, B. N.; vanSoolingen, D.; vanEmbden, J. D. A. Characterization of the catalase-peroxidase gene (*katG*) and *inhA* locus in isoniazid-resistant and -susceptible strains of *Mycobacterium tuberculosis* by automated DNA sequencing: restricted array of mutations associated with drug resistance. *J. Infect. Dis.* **1996**, *173*, 196–202.
(35) Rouse, D. A.; Li, Z.; Bai, G. H.; Morris, S. L. Characterization of the *katG* and *inhA* genes of isoniazid-resistant clinical isolates of *Mycobacterium tuberculosis*. *Antimicrob. Agents Chemother.* **1995**, *39*, 2472–2477.
(36) Milano, A.; De Rossi, E.; Gusberti, L.; Heym, B.; Marone, P.; Riccardi, G. The *katE* gene, which encodes the catalase HPII of *Mycobacterium avium*. *Mol. Microbiol.* **1996**, *19*, 113–123.
(37) Rozwarski, D. A.; Grant, G. A.; Barton, D. H.; Jacobs, W. R., Jr.; Sacchettini, J. C. Modification of the NADH of the isoniazid target (InhA) from *Mycobacterium tuberculosis*. *Science* **1998**, *279*, 98–102.
(38) Miesel, L.; Weisbrod, T. R.; Marcinkeviciene, J. A.; Bittman, R.; Jacobs, W. R., Jr. NADH dehydrogenase defects confer isoniazid resistance and conditional lethality in *Mycobacterium smegmatis*. *J. Bacteriol.* **1998**, *180*, 2459–2467.
(39) Basso, L. A.; Zheng, R.; Musser, J. M.; Jacobs, W. R., Jr.; Blanchard, J. S. Mechanisms of isoniazid resistance in *Mycobacterium tuberculosis*: enzymatic characterization of enoyl reductase mutants identified in isoniazid-resistant clinical isolates. *J. Infect. Dis.* **1998**, *178*, 769–775.
(40) Ramaswamy, S.; Musser, J. M. Molecular genetic basis of antimicrobial agent resistance in *Mycobacterium tuberculosis*: 1998 update. *Tuber. Lung Dis.* **1998**, *79*, 3–29.
(41) Dessen, A.; Quemard, A.; Blanchard, J. S.; Jacobs, W. R., Jr.; Sacchettini, J. C. Crystal structure and function of the isoniazid target of *Mycobacterium tuberculosis*. *Science* **1995**, *267*, 1638–1641.
(42) Morris, G. M.; Goodsell, D. S.; Huey, R.; Hart, W. E.; Halliday, S.; Belew, R.; Olson, A. J. *User Guide: AutoDock Version 3.0.5*; The Scripps Research Institute: La Jolla, 2001; p 85.
(43) Morris, G. M.; Goodsell, D. S.; Halliday, R. S.; Huey, R.; Hart, W. E.; Belew, R. K.; Olson, A. J. Automated docking using a Lamarckian genetic algorithm and an empirical binding free energy function. *J. Comput. Chem.* **1998**, *19*, 1639–1662.
(44) Case, D. A.; Darden, T. A.; Cheatham, T. E. I.; Simmerling, C. L.; Wang, J.; Duke, R. E.; Luo, R.; Merz, K. M.; Wang, B.; Pearlman, D. A.; Crowley, M.; Brozell, S.; Tsui, V.; Gohlke, H.; Mongan, J.; Hornak, V.; Cui, G.; Beroza, P.; Schafmeister, C.; Caldwell, J. W.; Ross, W. S.; Kollman, P. A. *AMBER8*; University of California: San Francisco, 2004.
(45) Duan, Y.; Wu, C.; Chowdhury, S.; Lee, M. C.; Xiong, G.; Zhang, W.; Yang, R.; Cieplak, P.; Luo, R.; Lee, T.; Caldwell, J.; Wang, J.; Kollman, P. A point-charge force field for molecular mechanics simulations of proteins based on condensed-phase quantum mechanical calculations. *J. Comput. Chem.* **2003**, *24*, 1999–2012.
(46) Cheatham, T. E.; Cieplak, P.; Kollman, P. A. A modified version of the Cornell *et al*. force field with improved sugar pucker phases and helical repeat. *J. Biomol. Struct. Dyn.* **1999**, *16*, 845–862.
(47) Jorgensen, W. L.; Chandrasekhar, J.; Madura, J. D.; Impey, R. W.; Klein, M. L. Comparison of simple potential functions for simulating liquid water. *J. Chem. Phys.* **1983**, *79*, 926–935.
(48) Berendsen, H. J. C.; Postma, J. P. M.; Vangunsteren, W. F.; Dinola, A.; Haak, J. R. Molecular-dynamics with coupling to an external bath. *J. Chem. Phys.* **1984**, *81*, 3684–3690.
(49) Ryckaert, J. P.; Ciccotti, G.; Berendsen, H. J. C. Numerical-integration of Cartesian equations of motion of a system with constraints-molecular-dynamics of n-alkanes. *J. Comput. Phys.* **1977**, *23*, 327–341.
(50) Sun, J. P.; Fedorov, A. A.; Lee, S. Y.; Guo, X. L.; Shen, K.; Lawrence, D. S.; Almo, S. C.; Zhang, Z. Y. Crystal structure of PTP1B complexed with a potent and selective bidentate inhibitor. *J. Biol. Chem.* **2003**, *278*, 12406–12414.
(51) Torshin, I. Molecular surface sequence analysis of several *E. coli* enzymes and implications for existence of casein kinase-2 bacterial predecessor. *Front. Biosci.* **1999**, *4*, D394–407.
(52) Wang, L. H.; Hingerty, B. E.; Srinivasan, A. R.; Olson, W. K.; Broyde, S. Accurate representation of B-DNA double helical structure with implicit solvent and counterions. *Biophys. J.* **2002**, *83*, 382–406.
(53) Feig, M.; Karanicolas, J.; Brooks, C. L., III. *MMTSB Tool Set*; MMTSB NIH Research Resource, The Scripps Research Institute: La Jolla, 2001.
(54) Coutinho, P. M.; Dowd, M. K.; Reilly, P. J. Automated docking of monosaccharide substrates and analogues and methyl alpha-acarviosinide in the glucoamylase active site. *Proteins* **1997**, *27*, 235–248.
(55) Sotriffer, C. A.; Flader, W.; Winger, R. H.; Rode, B. M.; Liedl, K. R.; Varga, J. M. Automated docking of ligands to antibodies: methods and applications. *Methods* **2000**, *20*, 280–291.
(56) Sotriffer, C. A.; Gohlke, H.; Klebe, G. Docking into knowledge-based potential fields: a comparative evaluation of DrugScore. *J. Med. Chem.* **2002**, *45*, 1967–1970.
(57) Claussen, H.; Buning, C.; Rarey, M.; Lengauer, T. FlexE: efficient molecular docking considering protein structure variations. *J. Mol. Biol.* **2001**, *308*, 377–395.
(58) Jones, G.; Willett, P.; Glen, R. C. Molecular recognition of receptor sites using a genetic algorithm with a description of desolvation. *J. Mol. Biol.* **1995**, *245*, 43–53.
(59) Kramer, B.; Rarey, M.; Lengauer, T. Evaluation of the FLEXX incremental construction algorithm for protein-ligand docking. *Proteins* **1999**, *37*, 228–241.
(60) Vieth, M.; Hirst, J. D.; Kolinski, A.; Brooks, C. L. Assessing energy functions for flexible docking. *J. Comput. Chem.* **1998**, *19*, 1612–1622.
(61) Ewing, T. J.; Makino, S.; Skillman, A. G.; Kuntz, I. D. DOCK 4.0: search strategies for automated molecular docking of flexible molecule databases. *J. Comput.-Aided. Mol. Des.* **2001**, *15*, 411–428.
(62) Sotriffer, C. A.; Flader, W.; Cooper, A.; Rode, B. M.; Linthicum, D. S.; Liedl, K. R.; Varga, J. M. Ligand binding by antibody IgE lb4: assessment of binding site preferences using microcalorimetry, docking, and free energy simulations. *Biophys. J.* **1999**, *76*, 2966–2977.
(63) Denessiouk, K. A.; Johnson, M. S. When fold is not important: a common structural framework for adenine and AMP binding in 12 unrelated protein families. *Proteins* **2000**, *38*, 310–326.
(64) Schroeder, E. K.; Basso, L. A.; Santos, D. S.; de Souza, O. N. Molecular dynamics simulation studies of the wild-type, I21V, and I16T mutants of isoniazid-resistant *Mycobacterium tuberculosis* enoyl reductase (InhA) in complex with NADH: toward the understanding of NADH-InhA different affinities. *Biophys. J.* **2005**, *89*, 876–884.
(65) Chen, Y. Z.; Gu, X. L.; Cao, Z. W. Can an optimization/scoring procedure in ligand-protein docking be employed to probe drug-resistant mutations in proteins. *J. Mol. Graphics Modell.* **2001**, *19*, 560–570.
(66) Pantano, S.; Alber, F.; Lamba, D.; Carloni, P. NADH interactions with WT- and S94A-acyl carrier protein reductase from *Mycobacterium tuberculosis*: an *ab initio* study. *Proteins* **2002**, *47*, 62–68.
(67) Aqvist, J.; Medina, C.; Samuelsson, J. E. A new method for predicting binding affinity in computer-aided drug design. *Protein Eng.* **1994**, *7*, 385–391.
(68) Beveridge, D. L.; DiCapua, F. M. Free energy via molecular simulation: applications to chemical and biomolecular systems. *Annu. Rev. Biophys. Biophys. Chem.* **1989**, *18*, 431–492.
(69) Kollman, P. Free energy calculations: applications to chemical and biochemical phenomena. *Chem. Rev.* **1993**, *93*, 2395–2417.
(70) Kollman, P. A.; Massova, I.; Reyes, C.; Kuhn, B.; Huo, S.; Chong, L.; Lee, M.; Lee, T.; Duan, Y.; Wang, W.; Donini, O.; Cieplak, P.; Srinivasan, J.; Case, D. A.; Cheatham, T. E. 3rd., Calculating structures and free energies of complex molecules: combining molecular mechanics and continuum models. *Acc. Chem. Res.* **2000**, *33*, 889–897.
(71) Bren, U.; Martinek, V.; Florian, J. Free energy simulations of uncatalyzed DNA replication fidelity: Structure and stability of T center dot G and dTTP center dot G terminal DNA mismatches flanked by a single dangling nucleotide. *J. Phys. Chem. B* **2006**, *110*, 10557–10566.

(72) Dolenc, J.; Baron, R.; Oostenbrink, C.; Koller, J.; van Gunsteren, W. F. Configurational entropy change of netropsin and distamycin upon DNA minor-groove binding. *Biophys. J.* **2006**, *91*, 1460–1470.

(73) Klauda, J. B.; Brooks, B. R. Sugar binding in lactose permease: Anomeric state of a disaccharide influences binding structure. *J. Mol. Biol.* **2007**, *367*, 1523–1534.

(74) Trzesniak, D.; Van Der Vegt, N. F. A.; Van Gunsteren, W. F. Analysis of neo-pentane-urea pair potentials of mean force in aqueous urea. *Mol. Phys.* **2007**, *105*, 33–39.

(75) Böhm, H. J. Prediction of binding constants of protein ligands: a fast method for the prioritization of hits obtained from de novo design or 3D database search programs. *J. Comput.-Aided Mol. Des.* **1998**, *12*, 309–323.

(76) Zagrovic, B.; van Gunsteren, W. F. Computational analysis of the mechanism and thermodynamics of inhibition of phosphodiesterase 5A by synthetic ligands. *J. Chem. Theory Comput.* **2007**, *3*, 301–311.

(77) Bren, M.; Florian, J.; Mavri, J.; Bren, U. Do all pieces make a whole? Thiele cumulants and the free energy decomposition. *Theor. Chem. Acc.* **2007**, *117*, 535–540.

(78) Wang, J.; Dixon, R.; Kollman, P. A. Ranking ligand binding affinities with avidin: a molecular dynamics-based interaction energy study. *Proteins* **1999**, *34*, 69–81.

(79) Wang, W.; Wang, J.; Kollman, P. A. What determines the van der Waals coefficient beta in the LIE (linear interaction energy) method to estimate binding free energies using molecular dynamics simulations. *Proteins* **1999**, *34*, 395–402.

(80) Ersmark, K.; Feierberg, I.; Bjelic, S.; Hultén, J.; Samuelsson, B.; Åqvist, J.; Hallberg, A. C_2-symmetric inhibitors of *Plasmodium falciparum* plasmepsin II: synthesis and theoretical predictions. *Bioorg. Med. Chem.* **2003**, *11*, 3723–3733.

(81) Florián, J.; Goodman, M. F.; Warshel, A. Computer simulations of protein functions: Searching for the molecular origin of the replication fidelity of DNA polymerases. *Proc. Natl. Acad. Sci. U.S.A.* **2005**, *102*, 6819–6824.

(82) Asi, A. M.; Rahman, N. A.; Merican, A. F. Application of the linear interaction energy method (LIE) to estimate the binding free energy values of *Escherichia coli* wild-type and mutant arginine repressor C-terminal domain (ArgRc)-L-arginine and ArgRc-L-citrulline protein-ligand complexes. *J. Mol. Graphics Modell.* **2004**, *22*, 249–262.

(83) Scior, T.; Meneses Morales, I.; Garces Eisele, S. J.; Domeyer, D.; Laufer, S. Antitubercular isoniazid and drug resistance of *Mycobacterium tuberculosis*--a review. *Arch. Pharm. (Weinheim)* **2002**, *335*, 511–525.

CI8001342